

Research Article

Safety Analysis against Tsunami Attacks at a Nuclear Power Plant Site

Jeong-Wook Seo, Jin Woo Lee, and Yong-Sik Cho

Department of Civil and Environmental Engineering, Hanyang University, 222 Wangsimni-ro, Seongdong-gu, Seoul 133-791, Republic of Korea

Correspondence should be addressed to Yong-Sik Cho; ysc59@hanyang.ac.kr

Received 21 June 2013; Revised 26 July 2013; Accepted 29 July 2013

Academic Editor: Mina Abd-El-Malek

Copyright © 2013 Jeong-Wook Seo et al. This is an open access article distributed under the Creative Commons Attribution License, which permits unrestricted use, distribution, and reproduction in any medium, provided the original work is properly cited.

Several nuclear power plants are now under operation, and more plants will be built along the eastern coast of the Korean Peninsula. These nuclear power plant sites may be vulnerable to unexpected tsunami attacks. In this study, a coupled numerical model based on the shallow-water theory was employed to analyze the safety of the Uljin Nuclear Power Plant site against three historical and eleven virtual tsunami attacks. The numerical model consisted of a transoceanic propagation and an inundation model. Both models were discretized by the finite difference method. Maximum and minimum tsunami heights were estimated for the three historical and eleven virtual tsunamis. The obtained results showed that the Uljin Nuclear Power Plant site would be safe against the tsunami attacks included in this study.

1. Introduction

Recently, several catastrophic tsunamis caused by undersea earthquakes have occurred around the Pacific Rim. These tsunamis are difficult to predict and can cause the loss of human life and property damage in coastal areas. According to a report by the National Oceanic and Atmospheric Administration (NOAA), one of the recent tsunamis occurred because of an earthquake near Sumatra, Indonesia, on December 26, 2004, and caused 227,898 human deaths and property damage of about 10 billion dollars. Another tsunami occurred because of an earthquake in Chile on February 27, 2010, causing 156 human deaths and property damage of about 30 billion dollars. A tsunami occurred because of the Great East Japan Earthquake on March 11, 2011, which resulted in almost 20,000 human deaths and missing persons and property damage of 210 billion dollars [1]. Among these tsunamis, the 2011 Great East Japan Tsunami (also called the 2011 Tohoku Tsunami) has attracted worldwide attention due to the casualty of the Fukushima Daiichi Nuclear Power Plant site and its ongoing crisis.

In the East Sea, surrounded by Korea, Japan, and Russia, three major tsunami events occurred in 1964, 1983, and 1993. In particular, the 1983 Central East Sea Tsunami caused huge

losses of human lives and property damage in Korean and Japanese coastal communities. Furthermore, according to a report of the Korea Meteorological Administration (KMA), the number of submarine earthquakes around the Korean Peninsula has recently increased: 23 times in 2008, 28 times in 2009, 18 times in 2010, 33 times in 2011, 28 times in 2012, and 34 times through June 2013 [2].

In Korea, several nuclear power plants are now under operation and more plants will be built along the eastern coast of the Korean Peninsula. These nuclear power plant sites may be vulnerable to unexpected tsunami attacks. Thus, in order to prevent unusual devastating damage from tsunamis, they are to be constructed in a safety zone along the coastline. A safety zone can be designated by using the maximum and minimum tsunami heights. Maximum tsunami heights can play a significant role in determination of the elevation of a nuclear power plant site, while minimum tsunami heights can be used to evaluate the safety of an essential service water system (ESWS), which is related to the reactor container, and a circulating water system (CWS) supplying the cooling water for the condenser. Fatal damage to nuclear power plant operation can occur when minimum tsunami heights are lower than the lowest allowable elevation of the essential service water pump. Thus, it is important to predict as

accurately as possible the maximum and minimum tsunami heights.

Because it is difficult to reproduce a tsunami by hydraulic modeling, studies regarding tsunamis have generally employed available numerical models. As discussed by Imamura et al. [3], a numerical model was developed by discretizing linear shallow-water equations with a leap-frog scheme in order to simulate the propagation of transoceanic tsunamis. This numerical model was improved by Cho and Yoon [4] in order to simulate the proper dispersive effects for tsunamis propagating obliquely to the principal axes of the computational grids. However, the numerical models of Imamura et al. and Cho and Yoon are limited to cases where there is a constant water depth if a uniform finite difference grid is employed. Therefore, both of the numerical models are limited in that the spatial grid size and time step size should be changed continuously in order to apply them to real topography. Yoon [5] also improved the numerical model of Cho and Yoon by using a uniform grid. However, this numerical model used a cubic interpolation function in order to calculate the value of the variables at a hidden grid point, and this can cause errors because of the many interpolation processes. Recently, a simple and practical numerical model using a dispersion-corrected scheme was developed by Cho et al. [6]. The model was based on a leap-frog scheme that was similar to the models of Imamura et al. and Cho and Yoon. However, the newly proposed model of Cho et al. is free of spatial grids and time step sizes, and the accuracy is better than that of Yoon's model due to the absence of the interpolation process. The accuracy of the scheme proposed by Cho et al. was also verified by Sohn et al. [7]. For this reason, the model of Cho et al. was used in the present study to simulate tsunami propagation and inundation.

In this study, the safety of the Uljin Nuclear Power Plant site against tsunami attacks is investigated by predicting the maximum and minimum tsunami heights. Three historical and eleven virtual tsunami events are employed to simulate the propagation of a tsunami across the East Sea. The eleven virtual tsunami events were first suggested by the Korea Peninsula Energy Development Organization (KEDO, 1999) to examine the safety of the Shinpo Nuclear Power Plant site in North Korea against tsunami attacks [8]. The numerical model for tsunami simulation, which is composed of a model for simulating the propagation of a tsunami across the East Sea and another model for simulating the run-up process of a tsunami, is based on the shallow-water theory.

2. Numerical Model for a Tsunami

2.1. Propagation Model. When tsunamis propagate over long distances, the dispersion effects may play an important role and should be considered in modeling. Thus, linear Boussinesq equations are adequate. The equations are given as

$$\frac{\partial \zeta}{\partial t} + \frac{\partial P}{\partial x} + \frac{\partial Q}{\partial y} = 0,$$

$$\begin{aligned} \frac{\partial P}{\partial t} + gh \frac{\partial \zeta}{\partial x} &= \frac{h^2}{2} \frac{\partial}{\partial x} \left[\frac{\partial}{\partial x} \left(\frac{\partial P}{\partial t} \right) + \frac{\partial}{\partial y} \left(\frac{\partial Q}{\partial t} \right) \right] \\ &\quad - \frac{h^3}{6} \frac{\partial}{\partial x} \left[\frac{\partial^2}{\partial t \partial x} \left(\frac{P}{h} \right) + \frac{\partial^2}{\partial t \partial y} \left(\frac{Q}{h} \right) \right], \\ \frac{\partial Q}{\partial t} + gh \frac{\partial \zeta}{\partial y} &= \frac{h^2}{2} \frac{\partial}{\partial y} \left[\frac{\partial}{\partial x} \left(\frac{\partial P}{\partial t} \right) + \frac{\partial}{\partial y} \left(\frac{\partial Q}{\partial t} \right) \right] \\ &\quad - \frac{h^3}{6} \frac{\partial}{\partial y} \left[\frac{\partial^2}{\partial t \partial x} \left(\frac{P}{h} \right) + \frac{\partial^2}{\partial t \partial y} \left(\frac{Q}{h} \right) \right], \end{aligned} \quad (1)$$

where ζ is the free surface displacement, P and Q are the depth-averaged volume fluxes in the x - and y -axis directions, respectively, g is the gravity acceleration, and h is the still water depth. After eliminating P and Q from (1), the linear Boussinesq equations are reduced over a constant depth as the following equation [9]:

$$\frac{\partial^2 \zeta}{\partial t^2} - gh \left(\frac{\partial^2 \zeta}{\partial x^2} + \frac{\partial^2 \zeta}{\partial y^2} \right) = \frac{\partial h^3}{3} \left(\frac{\partial^4 \zeta}{\partial x^4} + 2 \frac{\partial^4 \zeta}{\partial x^2 \partial y^2} + \frac{\partial^4 \zeta}{\partial y^4} \right). \quad (2)$$

The frequency dispersion term given by the right-hand side term of (2) is difficult to discretize, because of high order derivatives. If the frequency dispersion term is neglected, (2) is equal to a wave equation derived from the linear shallow-water equations. Thus, the linear shallow-water equations, instead of the linear Boussinesq equations, have been applied in previous studies and were therefore also applied to this study. The linear shallow-water equations can be written in the following form [10]:

$$\begin{aligned} \frac{\partial \zeta}{\partial t} + \frac{\partial P}{\partial x} + \frac{\partial Q}{\partial y} &= 0, \\ \frac{\partial P}{\partial t} + gh \frac{\partial \zeta}{\partial x} &= 0, \\ \frac{\partial Q}{\partial t} + gh \frac{\partial \zeta}{\partial y} &= 0. \end{aligned} \quad (3)$$

However, the linear shallow-water equations do not consider the dispersion effects. Thus, a dispersion-corrected scheme that can consider the dispersion effects is applied to the linear shallow-water equations [6]. The difference equations are represented as follows:

$$\begin{aligned} \frac{\zeta_{i,j}^{n+1/2} - \zeta_{i,j}^{n-1/2}}{\Delta t} + \frac{P_{i+1/2,j}^n - P_{i-1/2,j}^n}{\Delta x} + \frac{Q_{i,j+1/2}^n - Q_{i,j-1/2}^n}{\Delta y} &= 0, \\ \frac{P_{i+1/2,j}^{n+1} - P_{i+1/2,j}^n}{\Delta t} + gh_{i+1/2,j} \frac{\zeta_{i+1,j}^{n+1/2} - \zeta_{i,j}^{n+1/2}}{\Delta x} &= 0, \\ \frac{Q_{i,j+1/2}^{n+1} - Q_{i,j+1/2}^n}{\Delta t} + gh_{i,j+1/2} \frac{\zeta_{i+1,j}^{n+1/2} - \zeta_{i,j}^{n+1/2}}{\Delta y} &= 0. \end{aligned}$$

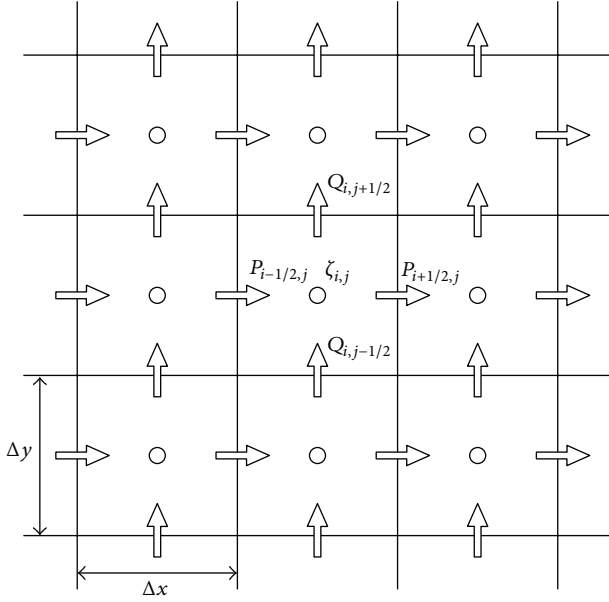


FIGURE 1: A sketch of the staggered grid system.

$$\begin{aligned}
& + \frac{\alpha}{12\Delta x} gh_{i+1/2,j} \left[\zeta_{i+2,j}^{n+1/2} - 3\zeta_{i+1,j}^{n+1/2} + 3\zeta_{i,j}^{n+1/2} - \zeta_{i-1,j}^{n+1/2} \right] \\
& + \frac{\gamma}{12\Delta x} gh_{i+1/2,j} \left[\left(\zeta_{i+1,j+1}^{n+1/2} - 2\zeta_{i+1,j}^{n+1/2} + \zeta_{i+1,j-1}^{n+1/2} \right) \right. \\
& \quad \left. - \left(\zeta_{i,j+1}^{n+1/2} - 2\zeta_{i,j}^{n+1/2} + \zeta_{i,j-1}^{n+1/2} \right) \right] = 0, \\
& \frac{Q_{i,j+1/2}^{n+1} - Q_{i,j+1/2}^n}{\Delta t} + gh_{i,j+1/2} \frac{\zeta_{i,j+1}^{n+1/2} - \zeta_{i,j}^{n+1/2}}{\Delta y} \\
& + \frac{\alpha}{12\Delta y} gh_{i,j+1/2} \left[\zeta_{i,j+2}^{n+1/2} - 3\zeta_{i,j+1}^{n+1/2} + 3\zeta_{i,j}^{n+1/2} - \zeta_{i,j-1}^{n+1/2} \right] \\
& + \frac{\gamma}{12\Delta y} gh_{i,j+1/2} \left[\left(\zeta_{i+1,j+1}^{n+1/2} - 2\zeta_{i,j+1}^{n+1/2} + \zeta_{i-1,j+1}^{n+1/2} \right) \right. \\
& \quad \left. - \left(\zeta_{i+1,j}^{n+1/2} - 2\zeta_{i,j}^{n+1/2} + \zeta_{i-1,j}^{n+1/2} \right) \right] = 0, \tag{4}
\end{aligned}$$

where α and γ are the dispersion-corrected coefficients. Because the staggered grid system is used, the free surface displacement is calculated in the center grid, and volume fluxes P and Q are calculated in the boundary grid. The staggered grid system is represented in Figure 1.

All terms in (4) are expanded using Taylor series expansion, and P and Q are eliminated. Then the equation for ζ is derived as follows [6]:

$$\begin{aligned}
& \frac{\partial^2 \zeta}{\partial t^2} - C_0^2 \left(\frac{\partial^2 \zeta}{\partial x^2} + \frac{\partial^2 \zeta}{\partial y^2} \right) - C_0^2 \frac{\Delta x^2}{12} (1 + \alpha - C_r^2) \\
& \quad \times \left(\frac{\partial^4 \zeta}{\partial x^4} + \frac{\partial^4 \zeta}{\partial x^2 \partial y^2} + \frac{\partial^4 \zeta}{\partial y^4} \right)
\end{aligned}$$

$$\begin{aligned}
& + (1 + \alpha - \gamma) C_0^2 \frac{\Delta x^2}{6} \frac{\partial^4 \zeta}{\partial x^2 \partial y^2} \\
& = O((\Delta x)^3, (\Delta x)^2 \Delta t, \Delta x (\Delta t)^2, (\Delta t)^3), \tag{5}
\end{aligned}$$

where $C_0 (= \sqrt{gh})$ and $C_r (= C_0 \Delta t / \Delta x)$ represent the phase velocity of a long wave and the Courant number, respectively. Comparing (5) with the linear Boussinesq equation (2), these equations are seen as identical as long as the following relations are satisfied. That is,

$$\alpha = \frac{4h^2 + gh\Delta t^2 - \Delta x^2}{\Delta x^2}, \quad \gamma = \alpha + 1. \tag{6}$$

The proposed scheme uses the numerical dispersion generated from the finite difference approximation to mimic the frequency dispersion term of the linear Boussinesq equations. Thus, even if the linear shallow-water equations are used to govern tsunami propagation, the application of the dispersion-corrected scheme results in numerical dispersion effects comparable to the physical dispersion effects of the linear Boussinesq equations [6].

2.2. Inundation Mode. As a tsunami approaches a coastal area where the depth is relatively shallow, the wavelength of the tsunami becomes shorter and the amplitude becomes larger. Thus, the nonlinear convective inertia force and bottom friction become increasingly important, while the significance of the frequency dispersion diminishes. To describe the flow motion in a coastal zone, nonlinear shallow-water equations are used [11] in the following form:

$$\begin{aligned}
& \frac{\partial \zeta}{\partial t} + \frac{\partial P}{\partial x} + \frac{\partial Q}{\partial y} = 0, \\
& \frac{\partial P}{\partial t} + \frac{\partial}{\partial x} \left(\frac{P^2}{H} \right) + \frac{\partial}{\partial y} \left(\frac{PQ}{H} \right) + gH \frac{\partial \zeta}{\partial x} + \tau_x H = 0, \tag{7} \\
& \frac{\partial Q}{\partial t} + \frac{\partial}{\partial x} \left(\frac{PQ}{H} \right) + \frac{\partial}{\partial y} \left(\frac{Q^2}{H} \right) + gH \frac{\partial \zeta}{\partial y} + \tau_y H = 0,
\end{aligned}$$

where H is the total water depth as $H = h + \zeta$ and τ_x and τ_y are bottom friction terms represented by the Manning equation. The equations can be written in the following form, where n is the Manning coefficient:

$$\begin{aligned}
& \tau_x = \frac{gn^2}{H^{10/3}} P (P^2 + Q^2)^{1/2}, \\
& \tau_y = \frac{gn^2}{H^{10/3}} Q (P^2 + Q^2)^{1/2}. \tag{8}
\end{aligned}$$

The linear terms of (7) are discretized by using the same method as (4), and the nonlinear terms are discretized by the upwind scheme. The finite difference scheme for the upwind scheme and a detailed description of the inundation model can be found in [12].

A moving boundary condition that can simulate the run-up process of tsunamis was implemented in the inundation

TABLE 1: The location of historical tsunamis occurrence and fault parameters.

Date	Location		H (km)	θ ($^\circ$)	δ ($^\circ$)	γ ($^\circ$)	L (km)	W (km)	D (km)	M
	Long. ($^\circ$ E)	Lat. ($^\circ$ N)								
June 16, 1964	139.42	38.74	1	189	56	90	80	30	3.30	7.5
May 26, 1983	138.84	40.21	2	22	40	90	40	30	7.60	7.7
	139.02	40.54	3	355	25	80	60	30	3.05	
	139.30	42.10	5	163	60	105	24.5	25	12.00	
July 12, 1993	139.25	42.34	5	175	60	105	30	25	2.50	7.8
	139.40	43.13	10	188	35	80	90	25	5.71	

TABLE 2: The location of virtual tsunamis occurrence and fault parameters.

Case	Location		H (km)	θ ($^\circ$)	δ ($^\circ$)	γ ($^\circ$)	L (km)	W (km)	D (km)	M
	Long. ($^\circ$ E)	Lat. ($^\circ$ N)								
Case 1	137.5	37.5		0.0						
Case 2	137.7	38.3		14.5						
Case 3	138.0	39.0		27.5						
Case 4	138.4	39.7		17.0						
Case 5	138.7	40.2		10.0						
Case 6	138.9	40.9	1	1.0	40	90	125.89	62.945	6.31	8.0
Case 7	139.0	41.7		1.0						
Case 8	139.1	42.1		4.0						
Case 9	139.1	42.9		2.0						
Case 10	139.2	43.5		2.0						
Case 11	139.2	44.4		3.0						

model. It is essential to use a fine grid mesh size that is smaller than 5 to 10 m in a simulation of the run-up process to get accurate results. However, the use of such a fine grid mesh size is prohibitive considering the computational time for modeling an area as large as the East Sea. Thus, the dynamic linking method should be used to obtain accuracy and computational efficiency with this kind of problem. In the dynamic linking method, coarser grids in the deep sea are dynamically linked with the grid that is 1/3 the size in the shallower region. During computation, the water level and discharge are exchanged with each other to satisfy the dynamic equilibrium. The process that composes and links each region of different grid sizes is iterated until the target area is described with proper resolution.

3. Numerical Simulation

3.1. Site Description. The Uljin Nuclear Power Plant is a large nuclear power station in the Gyeongsangbuk-do province of Korea. It is located at north latitude 37 degrees, 05 minutes, 34 seconds and east longitude 129 degrees, 23 minutes, 01 seconds. The facility has six pressurized water reactors (PWRs) with a total installed capacity of 5,881 MW. Since the Uljin Nuclear Power Plant started commercial operation on September 10, 1988, a great amount of electric power has been produced until now. At the present date, the Uljin Nuclear Power Plant is in charge of producing about 8% of the total electric power production in Korea. The location and panorama of the Uljin Nuclear Power Plant site are shown in Figure 2.

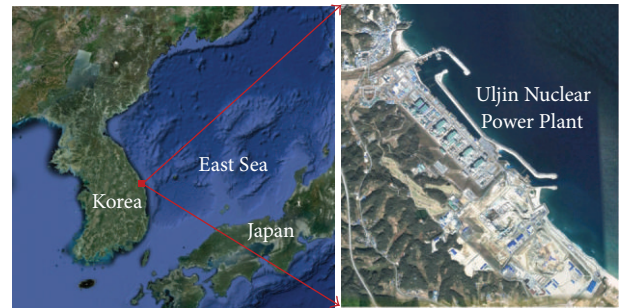


FIGURE 2: The location and panorama of the Uljin Nuclear Power Plant site (Google Earth 2013).

3.2. Initial Conditions. In this study, initial conditions for the tsunami simulation were three historical and eleven virtual tsunami events. The three historical tsunami events occurred in 1964, 1983, and 1993. The fault parameters of the three historical tsunamis have been proposed by prior researchers [13–15]. The Korean Peninsula Energy Development organization (KEDO) identified eleven points that have a high probability of the occurrence of an earthquake with magnitude 8.0 [8]. The locations of initial conditions for the tsunami simulation are represented in Figure 3. The locations and applied earthquake fault parameters of three historical and eleven virtual tsunamis are given in Tables 1 and 2, respectively. In the tables, H is the depth of the fault plane, θ is the strike angle, δ is the dip angle, γ is the slip

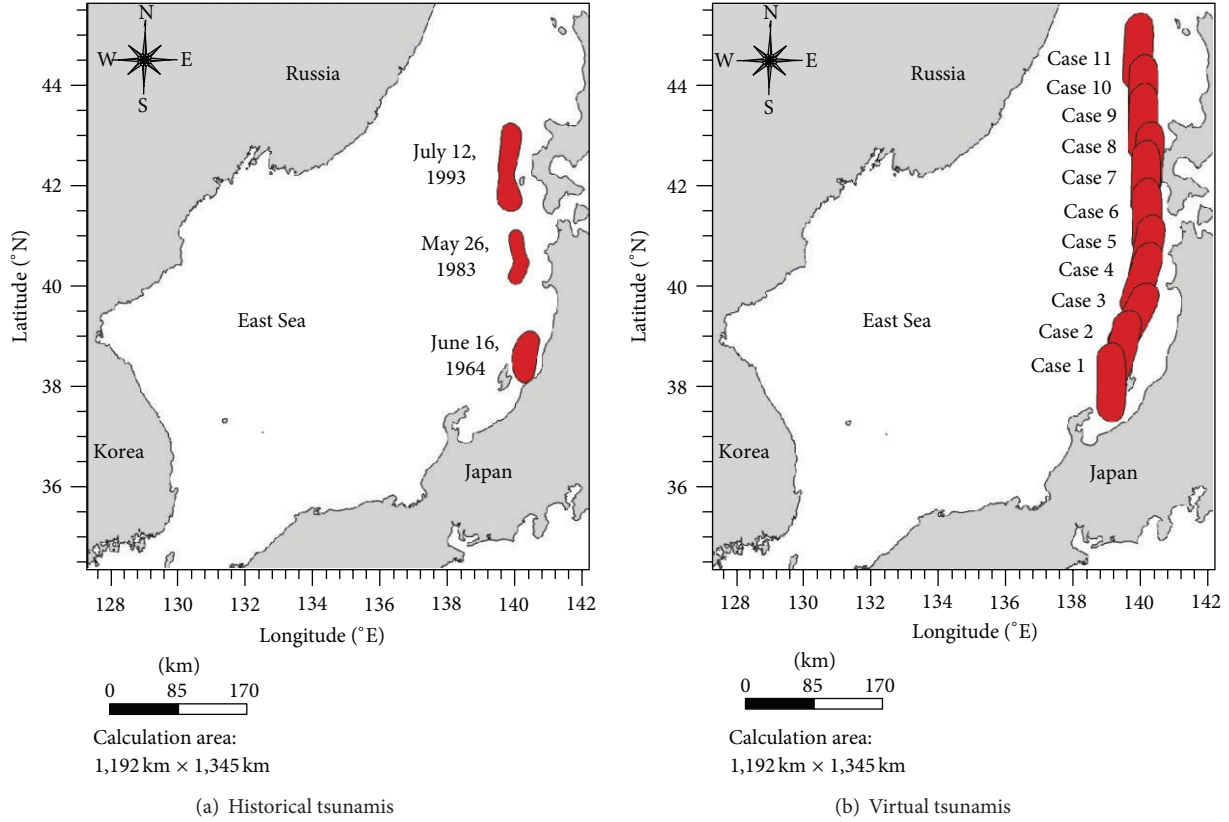


FIGURE 3: Locations of earthquake epicenters for historical and virtual tsunamis.

TABLE 3: Computational information for each region.

Region	Grid size ($\Delta x = \Delta y$)	Mesh number		Time step size (Δt)	Type of numerical model
		x	y		
A	1215.0 m	982	1,108	3.00000 sec	Linear
B	405.0 m	1,084	1,126	1.00000 sec	Linear
C	135.0 m	946	1,015	0.33333 sec	Linear
D	45.0 m	925	967	0.11111 sec	Linear
E	15.0 m	859	844	0.03704 sec	Nonlinear
F	5.0 m	778	697	0.03704 sec	Nonlinear

angle, L is the length of the fault, W is the width of the fault, D is the dislocation of the fault, and M is the magnitude of the earthquake. The length of the fault, the width of the fault, and the dislocation of the fault were obtained by using (9) proposed by the Korea Meteorological Administration (KMA). The depth of the fault plane, the dip angle, and the slip angle were obtained by using Mansinha and Smylie’s model [16]:

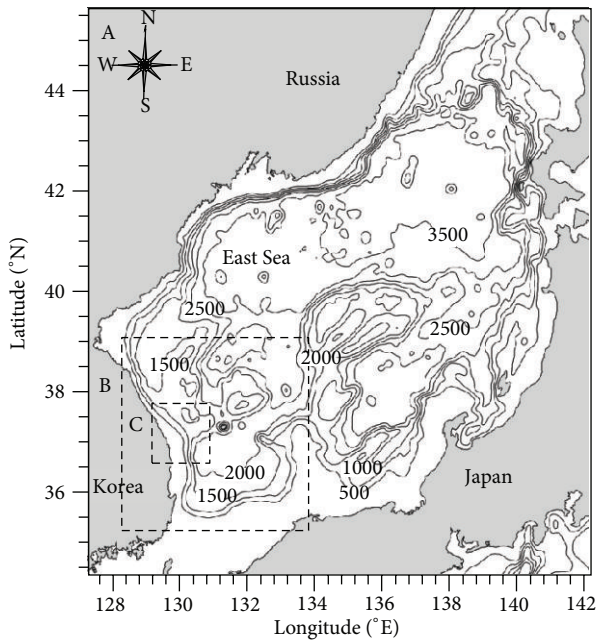
$$\begin{aligned} \log L &= 0.5M - 1.9, \\ W &= 0.5L, \\ \log D &= 0.5M - 1.2. \end{aligned} \tag{9}$$

3.3. *Nesting Scheme.* The computational domains covering the Uljin Nuclear Power Plant site are represented in Figure 4,

which shows each region and its bathymetry, including the East Sea. In order to investigate accurate inundation areas, region F was created using the measured elevation data. The numerical information and boundary conditions for each region are represented in Tables 3 and 4, respectively. As shown in Tables 3 and 4, the grid size was decreased by 1/3 according to the dynamic linking method. The free transmission condition was used for region A, and the dynamic linking method was used for the other regions as a boundary condition for the open sea. A fully reflected condition was used from region A to D, and the moving boundary condition was used for regions E and F as a boundary condition for land.

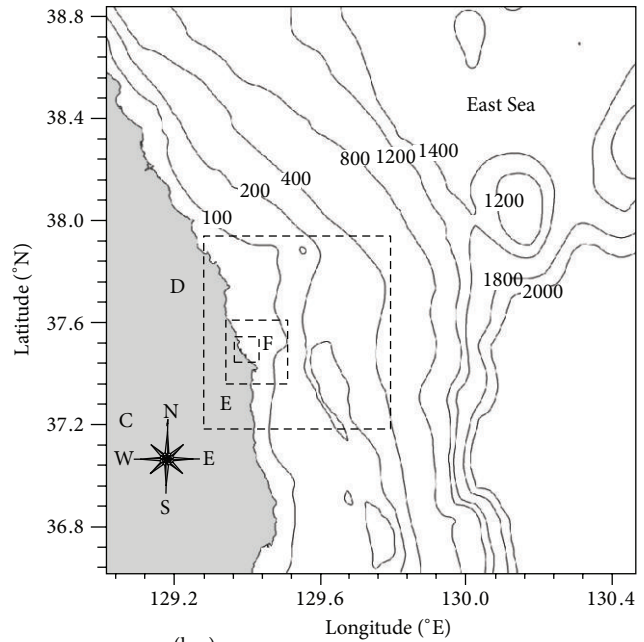
4. Results

In order to conduct an accurate safety analysis for the Uljin Nuclear Power Plant site, numerical simulations were carried



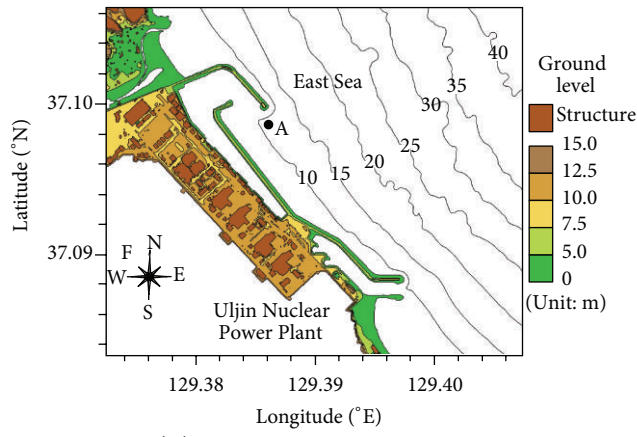
Calculation area:
1,192 km × 1,345 km

(a) Region A



Calculation area:
127.5 km × 136.9 km

(b) Region C



Calculation area:
3.09 km × 2.58 km

(c) Region F

FIGURE 4: Computational domain and bathymetry of the East Sea.

TABLE 4: Boundary condition for each region.

Region	A	B	C	D	E	F
Land	Fully reflected	Fully reflected	Fully reflected	Fully reflected	Moving boundary	Moving boundary
Open sea	Free transmission	Dynamic linking				

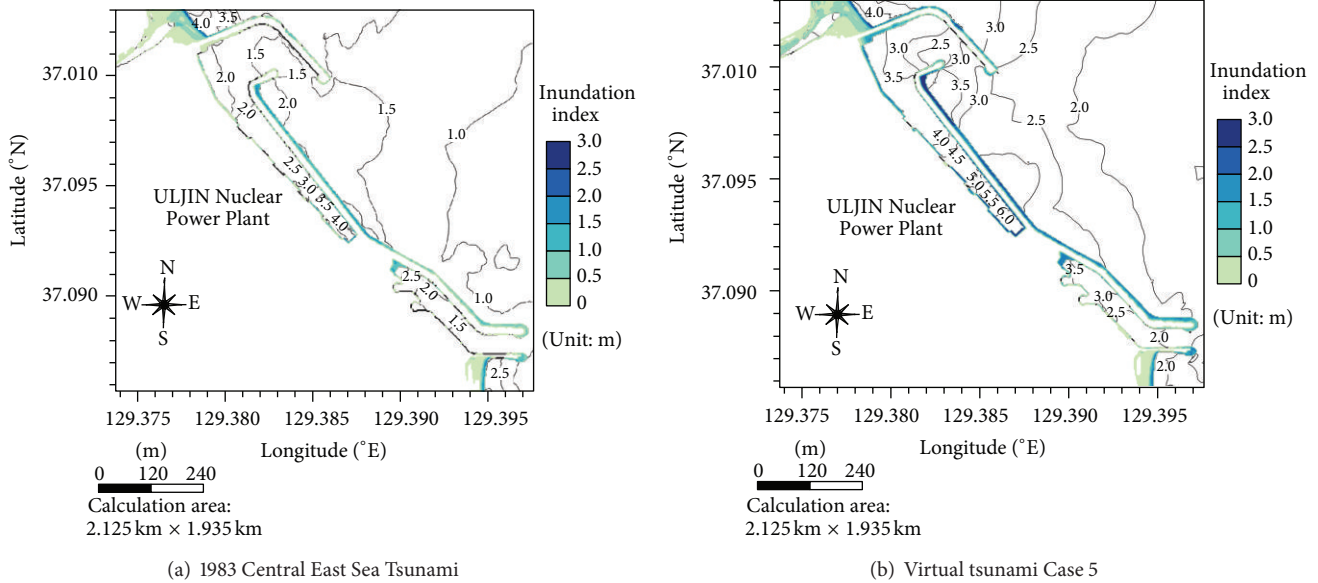


FIGURE 5: The maximum tsunami heights and inundation areas at each grid point.

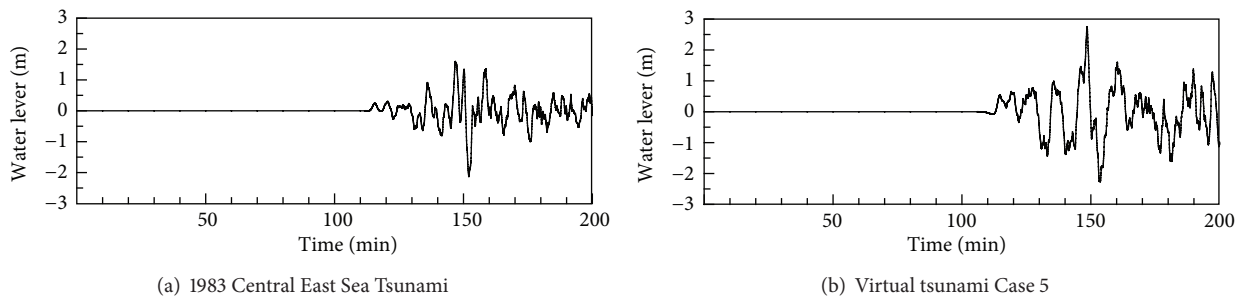


FIGURE 6: Time series of water levels at point A.

out for 200 minutes (3 hours, 20 minutes). Among the three historical and eleven virtual tsunamis, the Central East Sea Tsunami that occurred in 1983 and virtual tsunami Case 5 provided higher maximum tsunami heights than the others. Figure 5 represents the maximum tsunami heights and inundation areas obtained by numerical simulation at each point for those 2 cases. In order to observe the tsunami heights well inside the breakwater, region F was expanded in Figure 5. As shown in Figure 5, the location of the maximum tsunami heights for the 1983 tsunami and the Case 5 tsunami was generated at the most inner breakwater, and the maximum heights were approximately 4.4 m and 6.3 m, respectively. Inundation areas occurred at the rim of the breakwaters and the mouth of a river, which are located near the Uljin Nuclear Power Plant site. However, inundation areas for the 2 cases did not occur at the Uljin Nuclear Power Plant Site.

Figure 6 shows the time series of water levels at point A of region F for the 2 cases. The initial tsunami arrives about 110–120 minutes after the tsunami occurrence. In Case 5, the maximum amplitude up to 2.7 m could be found 40 minutes after the arrival of the first wave.

Figure 7 represents the minimum tsunami heights obtained by numerical simulation at each point for the 2 cases

and the locations of intake structures. As shown in Figure 7, the predicted minimum tsunami height from the numerical model is (–)6.5 m below mean sea level. However, because the minimum tsunami height is located at the edge of the breakwaters, it has nothing to do with the safety of intake structures. The main elevations of the Uljin Nuclear Power Plant site are shown in Figure 8. In comparison with the allowable lowest elevation of the essential water pump, the intake structures were evaluated to be safe for the minimum tsunami heights.

5. Conclusion

In this study, a composite numerical model based on linear shallow-water equations was employed to analyze the safety of the Uljin Nuclear Power Plant site against three historical and eleven virtual tsunami attacks. The numerical model was computationally efficient through the use of the linear shallow-water equations and dynamic linking method, which allowed for the selection of different mesh sizes within the computational domain.

The results of the numerical simulations for three historical and eleven virtual tsunamis showed that the Uljin

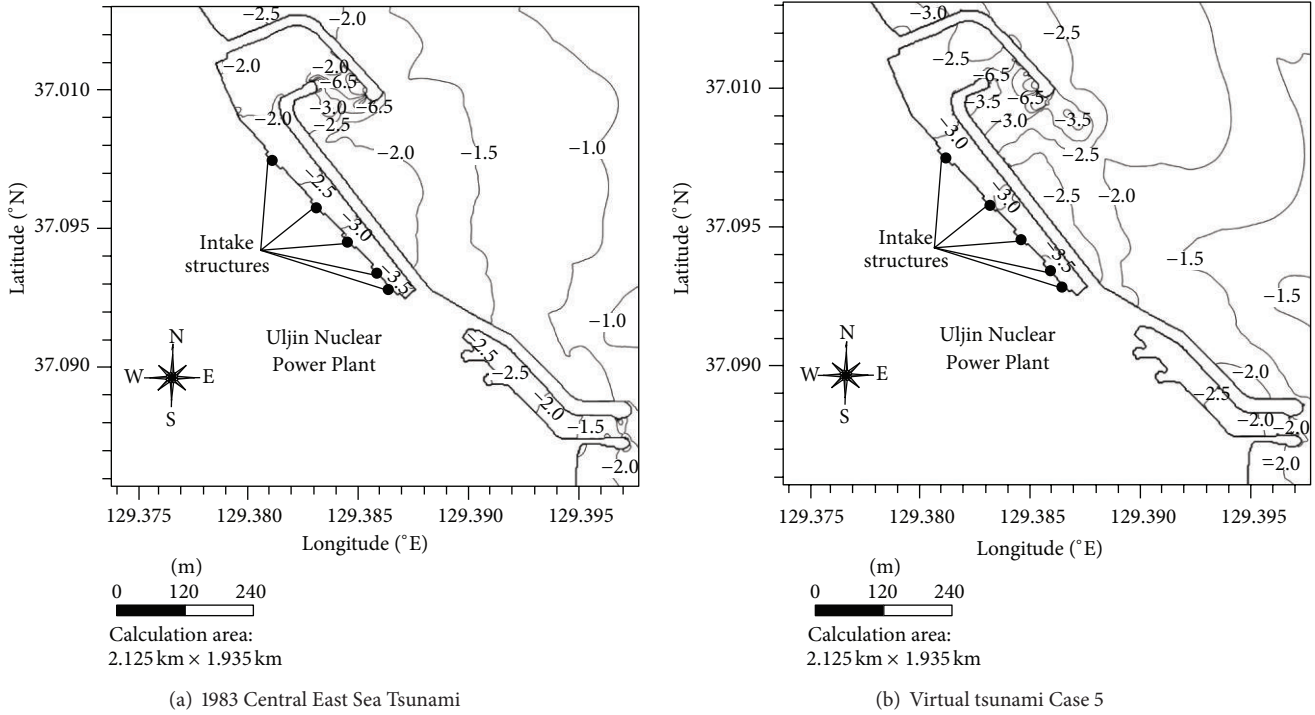


FIGURE 7: The minimum tsunami heights at each grid point.

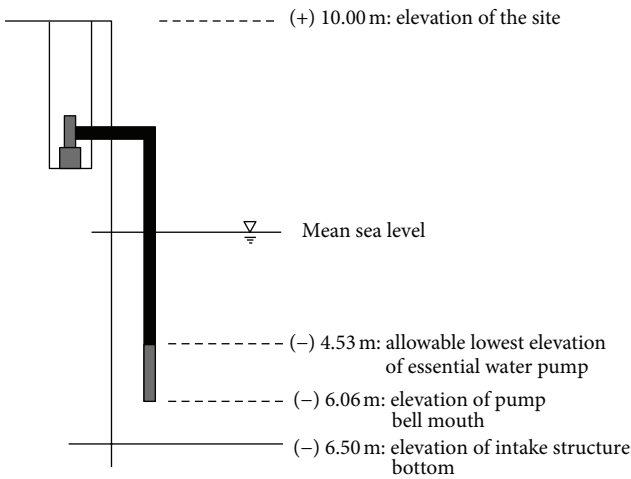


FIGURE 8: Main elevations of the Uljin Nuclear Power Plant site.

Nuclear Power Plant site is safe, at least against those tsunami events. By taking into consideration the elevation of the Uljin Nuclear Power Plant site, it can be concluded that the site is safe from those tsunami attacks.

Acknowledgment

This research was supported by the Research Program through the National Research Foundation of Korea funded by the Ministry of Education, Science and Technology (no. 2011-0015386).

References

- [1] National Oceanic and Atmospheric Administration, "Tsunami Event Database," <http://www.ngdc.noaa.gov/hazard/hazards.shtml>, 2013.
- [2] Korea Meteorological Administration, "Tsunami Event Database," <http://www.kma.go.kr/wheather/earthquake/domesticlist.jsp>, 2013.
- [3] F. Imamura, N. Shuto, and C. Goto, "Numerical simulations of the transoceanic propagation of tsunamis," in *Proceedings of the 6th Congress Asian and Pacific Regional Division (IAHR '88)*, pp. 265–272, Kyoto, Japan, 1988.
- [4] Y.-S. Cho and S. Yoon, "A modified leap-frog scheme for linear shallow-water equations," *Coastal Engineering Journal*, vol. 40, no. 2, pp. 191–205, 1998.
- [5] S. Yoon, "Propagation of distant tsunamis over slowly varying topography," *Journal of Geophysical Research C*, vol. 107, no. 10, pp. 4(1)–1(11), 2002.
- [6] Y.-S. Cho, D. Sohn, and S. O. Lee, "Practical modified scheme of linear shallow-water equations for distant propagation of tsunamis," *Ocean Engineering*, vol. 34, no. 11-12, pp. 1769–1777, 2007.
- [7] D.-H. Sohn, T. Ha, and Y.-S. Cho, "Distant tsunami simulation with corrected dispersion effects," *Coastal Engineering Journal*, vol. 51, no. 2, pp. 123–141, 2009.
- [8] Korean peninsula Energy Development Organization, *Estimation of Tsunami Height For KEDO LWR Project*, Korea Power Engineering Company, Seoul, Republic of Korea, 1999.
- [9] C. C. Mei, *The Applied Dynamics of Ocean Surface Waves*, World Scientific, River Edge, NJ, USA, 1989.
- [10] P. L.-F. Liu, Y.-S. Cho, S. Yoon, and S. N. Seo, "Numerical simulations of the 1960 Chilean Tsunami propagation and inundation at Hilo, Hawaii," in *Tsunami: Progress in Prediction*,

- Disaster Prevention and Warning*, Y. Tsuchiya and N. Shuto, Eds., pp. 99–115, Kluwer Academic Publisher, Boston, Mass, USA, 1994.
- [11] K. Kajiura and N. Shuto, “Tsunami,” in *The Sea*, B. Le Mehaute and D. M. Hanes, Eds., vol. 9, part B, pp. 395–420, John Wiley & Sons, New York, NY, USA, 1990.
- [12] Y.-S. Cho, *Numerical simulations of tsunami propagation and run-up [Ph.D. thesis]*, Cornell University, Ithaca, NY, USA, 1995.
- [13] I. Aida, “A source models of the 1983 Nihonkai-earthquake tsunami,” in *Proceedings of the Symposium on Nihonkai Chubu Earthquake Tsunami*, pp. 9–21, Japan Society of Civil Engineers (JSCE), 1984.
- [14] R. Sato, K. Abe, Y. Okada, K. Shinazake, and Y. Suzuki, *Handbook of Earthquake Fault Parameters in Japan*, kajima shuppankai, Tokyo, Japan, 1989.
- [15] T. Takahashi, N. Shuto, F. Imamura, and M. Oritiz, “The best fault model for the 1993 Hokkaido Nansei-oki Earthquake Tsunami,” in *Proceeding of the Coastal Engineering Conference*, vol. 41, pp. 251–255, 1994.
- [16] L. Mansinha and D. E. Smylie, “The displacement fields of inclined faults,” *Bulletin of the Seismological Society of America*, vol. 61, no. 5, pp. 1433–1440, 1971.